EJN European Journal of Neuroscience

FENS Federation of European Neuroscience Societies

European Journal of Neuroscience, Vol. 41, pp. 748–759, 2015 doi:10.1111/ejn.12822

NEUROSYSTEMS

Identification of a direct GABAergic pallidocortical pathway in rodents

Michael C. Chen,[1] Loris Ferrari,[1] Matthew D. Sacchet,[2,3] Lara C. Foland-Ross,[2] Mei-Hong Qiu,[1,4] Ian H. Gotlib,[2,3] Patrick M. Fuller,[1] Elda Arrigoni[1] and Jun Lu[1]

[1]Department of Neurology, Beth Israel Deaconess Medical Center and Harvard Medical School, 3 Blackfan Circle, CLS 717, Boston, MA 02115, USA

[2]Department of Psychology, Stanford University, Stanford, CA, USA

[3]Neurosciences Program, Stanford University, Stanford, CA, USA

[4]State Key Laboratory of Medical Neurobiology, Shanghai Medical College, Fudan University, Shanghai, China

Keywords: basal ganglia, frontal cortex, GABA, globus pallidus

Abstract

Interaction between the basal ganglia and the cortex plays a critical role in a range of behaviors. Output from the basal ganglia to the cortex is thought to be relayed through the thalamus, but an intriguing alternative is that the basal ganglia may directly project to and communicate with the cortex. We explored an efferent projection from the globus pallidus externa (GPe), a key hub in the basal ganglia system, to the cortex of rats and mice. Anterograde and retrograde tracing revealed projections to the frontal premotor cortex, especially the deep projecting layers, originating from GPe neurons that receive axonal inputs from the dorsal striatum. Cre-dependent anterograde tracing in Vgat-ires-cre mice confirmed that the pallidocortical projection is GABAergic, and *in vitro* optogenetic stimulation in the cortex of these projections produced a fast inhibitory postsynaptic current in targeted cells that was abolished by bicuculline. The pallidocortical projections targeted GABAergic interneurons and, to a lesser extent, pyramidal neurons. This GABAergic pallidocortical pathway directly links the basal ganglia and cortex, and may play a key role in behavior and cognition in normal and disease states.

Introduction

The basal ganglia are a collection of heterogeneous forebrain structures that play a critical role in motor behavior, cognition, affect, and sleep–wake regulation. One model of basal ganglia function proposes direct and indirect pathways for processing cortical information within the basal ganglia for output back to the cortex (Albin *et al.*, 1989). In both pathways, the basal ganglia output to the cortex occurs via thalamic relays, either directly from the striatum to the globus pallidus interna (GPi) and the substantia nigra reticulata (SNr), or indirectly via the globus pallidus externa (GPe), the subthalamic nucleus (STN), and the GPi/SNr. This model of basal ganglia function provides an interpretative framework for understanding the etiology and pathogenesis of such disorders as Parkinson's disease, but it is insufficient to explain many pathological features of these diseases (Obeso *et al.*, 2008).

Basal ganglia structures such as the GPe have robust connections within the basal ganglia, receiving striatal and subthalamic inputs and projecting back to these structures and the SNr and GPi, connecting every input and output structure of the basal ganglia (Kita, 2007). Basal ganglia outputs to the cortex, however, are thought to be primarily mediated by basal ganglia–thalamus–cortex relays. Deep brain stimulation of the STN and GPe ameliorates the symptoms of Parkinson's disease (Vitek *et al.*, 2012), but stimulation of the thalamus, the putative output relay for the basal ganglia, improves tremor but not necessarily bradykinesia and rigidity (Fasano *et al.*, 2012). Studies of the role of the basal ganglia in sleep add further complexity to the interaction of basal ganglia structures and other brain regions. Lesions of the GPe, but not of the STN or SNr, produce profound increases in wakefulness and alter motor behavior in rats (Qiu *et al.*, 2010). In contrast, lesions of the thalamus have a minimal effect on overall sleep–wake patterns (Fuller *et al.*, 2011). These findings suggest the intriguing hypothesis that the basal ganglia, specifically the GPe, project to and directly communicate with other structures in the brain to influence behavior. Retrograde tracing from the cortex has previously identified neurons located in the GPe projecting to the cortex, but no study has shown that these are GPe neurons of the basal ganglia, rather than basal forebrain (BF) cortically projecting neurons (Saper, 1984; Zaborszky *et al.*, 2013). GABAergic GPe neurons projecting directly to the cortex would denote a novel basal ganglia output pathway with a potentially unique role in regulating motor and premotor cortical activity.

To investigate the efferent projection targets of the GPe, we performed unilateral injections of an adeno-associated viral vector (AAV) expressing a channelrhodopsin-2 (ChR2)–yellow fluorescent protein (YFP) fusion product into the GPe of rats. We combined

Correspondence: Michael C. Chen and Jun Lu, as above.
E-mails: mcchen@alumni.stanford.edu and jlu@bidmc.harvard.edu

Received 18 November 2014, revised 1 December 2014, accepted 2 December 2014

retrograde and anterograde tracing to confirm that the pallicortical pathway originates from GPe neurons, and we used AAV–ChR2 in Vgat-ires-cre mice to specify and differentiate novel GPe projections. Finally, we used *in vitro* optogenetic stimulation of these GABAergic GPe projections to explore their functional role in cortical control.

Materials and methods

Tracer injections

Twelve adult male Sprague-Dawley rats, weighing 300–325 g (Taconic, Hudson, NY, USA), and five adult female Vgat-ires-cre mice (Vong *et al.*, 2011), weighing 20–25 g, were used. Rats were individually housed, and mice were group-housed, in temperature-controlled and humidity-controlled rooms, under 12 : 12-h light–dark cycles with *ad libitum* access to food and water. Animal care was in accordance with National Institutes of Health standards, with measures to minimise pain and discomfort, and all procedures used were approved by the Beth Israel Deaconess Medical Center Institutional Animal Care and Use Committee. Rats and mice were weighed, anesthetised with an intraperitoneal injection of a ketamine (100 mg/kg)–xylazine (10 mg/kg) mixture, and placed into a stereotaxic frame. The cranium was exposed for measurement of coordinates relative to bregma, and a burr hole was made for injections. A 1-mm glass pipette with a 10–20-μm tapered tip was inserted into the brain at the calculated coordinates. Injections were performed with electronically controlled air puffs lasting for 5–10 ms at 1–2 Hz. Injection volume was determined by measuring the meniscus of the injection liquid within the pipette by use of calibrated reticules on a surgical microscope. After 5 min of waiting to prevent backflow, the pipette was raised. After all injections, the scalp wound was closed with surgical clips, and the rodents were given meloxicam (5 mg/kg) subcutaneously once daily for 2 days.

We used at least five rodents in each tracing group to ensure consistency of the neuroanatomical pathways described; none of the rodents had undergone any previous procedures. In six rats, we performed unilateral injections (24 nL) of elongation factor-1 alpha (EF1a)–humanised ChR2 (hChR2) (H134R)–enhanced YFP (eYFP)–AAV10 into the GPe [AP = −1.0 mm, ML = −3.2 mm, DV = −5.2 mm (Paxinos & Watson, 2005)]. In six rats, we performed unilateral injections of fluorogold (120 nL) into frontal area 2 (Fr2) (AP = 3.2 mm, ML = 2.0 mm, DV = −1 mm), and, in two of these rats, unilateral injections of biotinylated dextran amine (45 nL) into the dorsal striatum [caudate putamen (CPu)] (AP = −1.7 mm, ML = 2.8 mm, DV = −4.2 mm). For mice, we performed unilateral injections (15 nL) of EF1a–double-floxed inverse ORF (DIO)–hChR2 (H134R)–eYFP–AAV10 into the GPe [AP = −0.35 mm, ML = −1.8 mm, DV = −3.3 mm (Franklin & Paxinos, 2008)]. All AAV–hChR2 (H134R)–YFP vectors were generously provided by K. Deisseroth, and were packaged into AAV10. The vector stocks were titered by real-time polymerase chain reaction with an Eppendorf Realplex machine. The titer of the preparations ranged from approximately 1×10^{12} to 1×10^{13} vector genomes copies/mL.

Immunohistochemistry

At least 2 weeks after injection, animals were deeply anesthetised with 7% chloral hydrate and perfused with 10% buffered formalin (Fisher Scientific, Pittsburgh, PA, USA). Brains were transferred to a solution of 20% sucrose and phosphate-buffered saline containing 0.02% sodium azide overnight, and then sliced into four series of 40-μm sections with a freezing microtome. For staining, we incubated tissue in primary polyclonal anti-green fluorescent protein (GFP) 1 : 20 000 (Invitrogen; A-6455, Lot 622086) or anti-fluorogold 1 : 10 000 (Chemikon; AB153) for 24 h, and then in biotinylated secondary antiserum in phosphate buffered saline with Triton-×100 (PBST) (Vector Laboratories) for 1 h. After being washed with phosphate-buffered saline, tissue was incubated with an avidin–biotin–horseradish peroxidase conjugate (Vector Laboratories), and stained brown with 0.05% 3,3′-diaminobenzidine tetrahydrochloride (Sigma, St Louis, MO, USA) and 0.02% H_2O_2, or black with 0.05% cobalt chloride and 0.01% nickel ammonium sulfate. Sections were then mounted onto slides [some sections were stained with 0.1% Thionin (Sigma)], dehydrated, and coverslipped.

Grayscale figures were obtained in monochrome with a blue filter in ADOBE PHOTOSHOP, which minimises the blue channel dominated

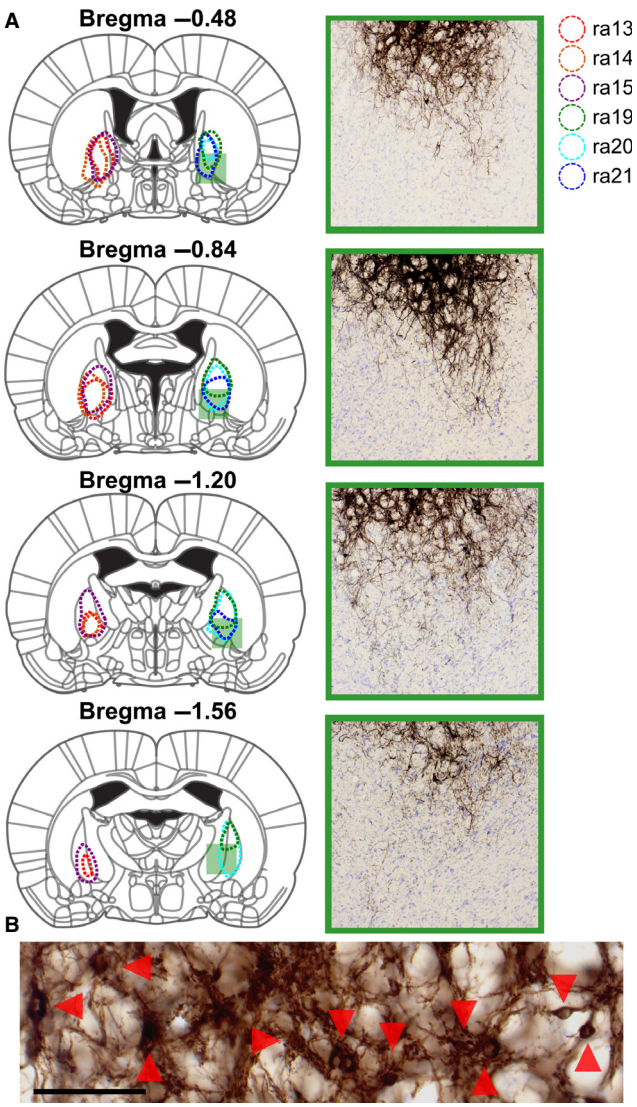

FIG. 1. Sites of injection of ChR2 into the rat GPe overlaid onto a standard rat atlas. (A) All injections were unilateral, and injection outlines are split between sides for visibility. Boxes, corresponding to case ra19, show a magnified image of the green square zones on the injection diagram. Magnified images show injections in the GPe and extensive fibers, with no filled cell bodies in the BF. (B) Filled cell bodies in the GPe injection site. Scale bar: 100 μm.

by the thionin Nissl staining while preserving the black or brown staining for better visualisation of projections from the injection site. To quantify staining intensity, we inverted the grayscale figures, marked the cortical subregion boundaries, and measured the pixel intensity in IMAGEJ on a 200-pixel line drawn from the edge of the cortex to the white matter in each cortical subregion. The intensity was normalised to the average of all measured subregions, and the distance from edge of the cortex was normalised to each measurement.

Whole cell in vitro *experiments*

Vgat-ires-cre, lox-GFP (n = 7) mice (8 weeks, 20–25 g) were used for *in vitro* electrophysiological recordings. This number of mice was used to allow successful recording of a sufficient number of Fr2 neurons to functionally characterise the pallidocortical pathway. EF1a–DIO–hChR2 (H134R)–eYFP–AAV10 (15 nL) was injected bilaterally in the GPe (AP = −0.35 mm, ML = −1.8 mm, DV = −3.3 mm). Four weeks after these injections, mice were used for *in vitro* electrophysiological recordings. Mice were anesthetised (150 mg/kg ketamine and 15 mg/kg xylazine, intraperitoneal) and transcardially perfused with ice-cold artificial cerebrospinal fluid (*N*-methyl-D-glucamine-based solution) containing: 100 mM *N*-methyl-D-glucamine chloride, 2.5 mM KCl, 1.24 mM NaH_2PO_4, 30 mM $NaHCO_3$, 20 mM HEPES, 25 mM glucose, 2 mM thiourea, 5 mM sodium ascorbate, 3 mM sodium pyruvate, 0.5 mM $CaCl_2$, and 10 mM $MgSO_4$ (adjusted to pH 7.3 with HCl when carbogenated with 95% O_2 and 5% CO_2). Their brains were quickly removed and cut into coronal frontal cortical slices (thickness, 250 μm) with a vibrating microtome (VT1000; Leica, Bannockburn, IL, USA). Slices containing Fr2 were transferred to normal artificial cerebrospinal fluid (sodium-based solution) containing: 120 mM NaCl, 2.5 mM KCl, 10 mM glucose, 26 mM $NaHCO_3$, 1.24 mM NaH_2PO_4, 1.3 mM $MgCl_2$, 4 mM $CaCl_2$, 2 mM thiourea, 1 mM sodium ascorbate, 3 mM sodium pyruvate, and 1 mM kynurenic acid (pH 7.4 when carbogenated with 95% O_2 and 5% CO_2, 310–320 mOsm).

Recordings were made from 17 GFP-positive and 19 pyramidal cells in the deep layers (V/VI) of the Fr2 premotor cortex from seven mice. On average, five neurons per mouse were recorded (ranging from 4–7 per mouse). Recordings were guided with a combination of fluorescence and infrared (IR) differential interference contrast video microscopy and a fixed-stage upright microscope (BX51WI; Olympus America) equipped with a Nomarski water immersion lens (×40/0.8 W) and IR-sensitive CCD camera (ORCA-ER; Hamamatsu, Bridgewater, NJ, USA), and images were displayed on a computer screen in real time by the use of AXIOVISION software (Carl Zeiss MicroImaging). Recordings were conducted in whole cell configuration at room temperature with a Multiclamp 700B amplifier (Molecular Devices, Foster City, CA, USA), a Digidata 1322A interface, and CLAMPEX 9.0 software (Molecular Devices). Globus pallidus axons and synaptic terminals expressing ChR2 were activated by full-field 5-ms flashes of light (~10 mW/mm^2, 1-mm beamwidth) from a 5-W luxeon blue-light-emitting diode (wavelength, 470 nm; #M470L2-C4; Thorlabs, Newton, NJ, USA) coupled to the epifluorescence pathway of the Zeiss microscope. The area stimulated included the recorded cell, which is in

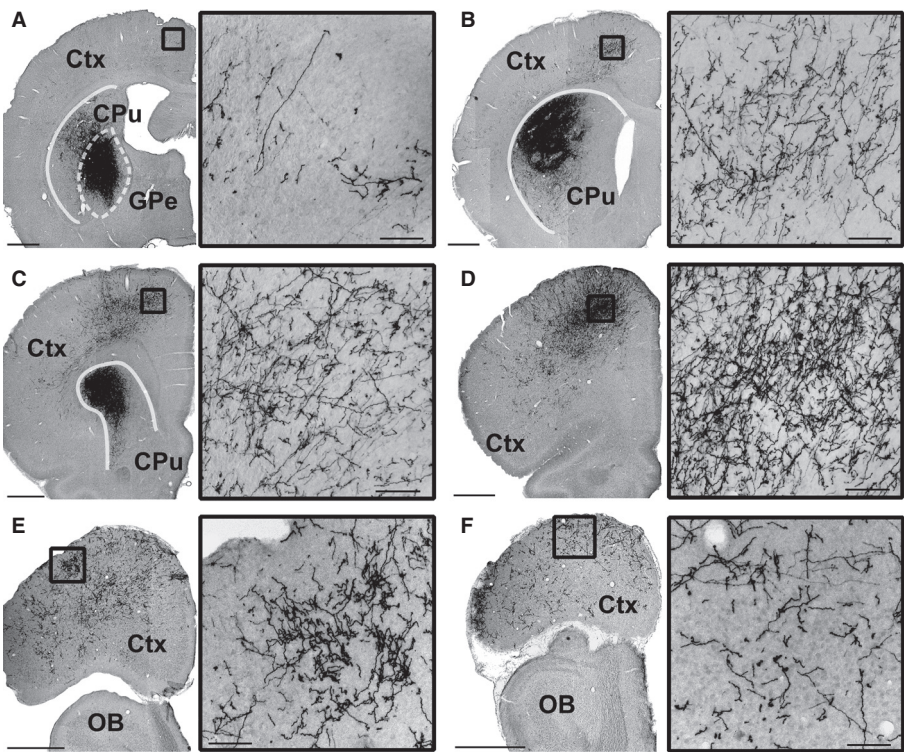

FIG. 2. Tracer injection into the GPe, stained black against GFP, labels projections to the Fr2 cortex at levels rostral to the injection site. (A) At the level of the injection site, heavy staining is observed in the dorsal striatum, whereas sparse projections and terminals can be seen in the caudal extent of Fr2 (inset). (B) At the rostrocaudal level of the striatum, GPe projections into the striatum and Fr2 are seen (inset). (C) At the level of the rostral striatum, heavy GPe projections to both the striatum and Fr2 are seen, with dense fibers and terminals throughout layers V and VI. (D–F) GPe projections reached their heaviest level at the rostral extent of the striatum (D), with dense fibers and terminals through all layers (inset), while expanding laterally through the cortex (E) and reaching the most rostral extent of the cortex (F). Ctx, cortex; OB, olfactory bulb. Scale bars: 1 mm; insets 100 μm.

the center of a 500-μm-radius concentric field. Photo-evoked inhibitory postsynaptic currents (IPSCs) were recorded at V_h = −40 mV in a potassium gluconate-based pipette solution containing: 120 mM potassium gluconate, 10 mM KCl, 10 mM HEPES, 3 mM $MgCl_2$, 5 mM K-ATP, 0.3 mM Na-GTP, and 0.5% biocytin (pH adjusted to 7.2 with KOH, 280 mOsm). The liquid junction potential was calculated to be +13.2 mV, and no recordings were corrected for it.

Electrophysiological data were analysed with CLAMPFIT 9.0 (Molecular Devices) and IGOR PRO 6 (WaveMetrics, Lake Oswego, OR, USA). Synaptic events were detected off-line with MINI ANALYSIS 6 (Synaptosoft, Leonia, NJ, USA). Action potential duration was calculated as the width at the voltage halfway between the action potential threshold and the action potential peak, and action potential threshold was calculated as the voltage at which the slope of the action potential reached ≥20 V/s. The latency of the photo-evoked IPSCs was determined from the time difference between the start of the light pulse and the 5% rise point of the first IPSC. Results are expressed as mean ± standard error of the mean (SEM), and *n* refers to the number of cells. Immediately following the *in vitro* recordings, recorded slices and slices containing the injection site were fixed in 10% buffered formalin (overnight), and then cryoprotected in 40% sucrose and re-sectioned into 60-μm sections on a freezing microtome. We examined the sections under fluorescence to verify the location and extent of ChR2–YFP-expressing neurons in the injection sites, as the GPe injection site clearly showed dense fibers and terminals in addition to the native GFP fluorescence. We

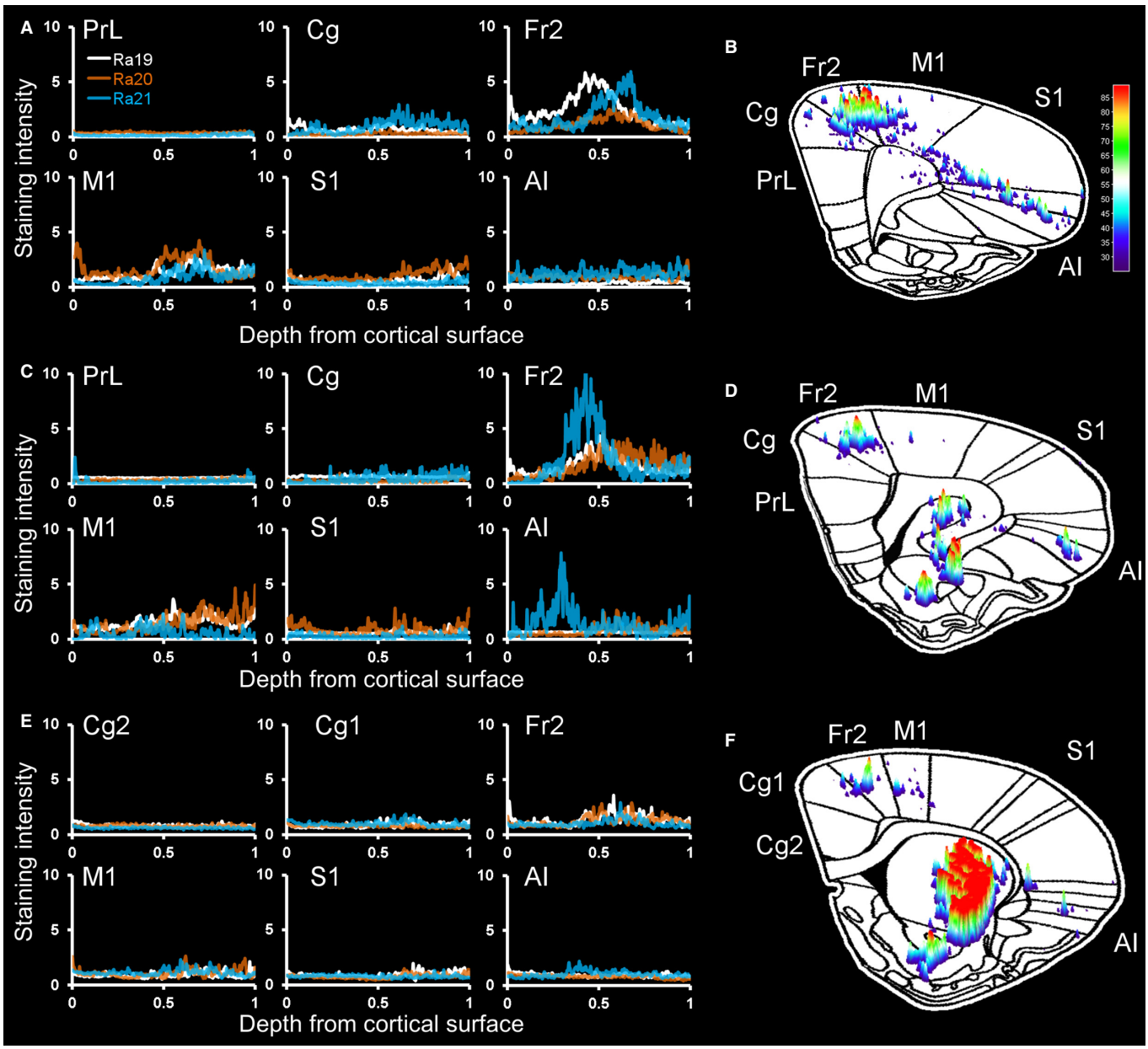

FIG. 3. Quantitative mapping of GPe projections to cortical subregions in rats. (A, C, and E) Projection mapping in three representative rat cases, with plotting of normalised staining intensity against relative distance from the cortical surface to the white matter. (B, D, and F) Projection intensity from case ra21 overlaid on a standardised mouse atlas demonstrates the typical pattern of the GABAergic pallidocortical projection, with heavy projections to Fr2 and adjacent areas. Staining intensities of six major cortical areas are presented at the level anterior to the striatum (A and B), the anterior striatum (C and D), and the striatum (E and F). AI, anterior insula; Cg, cingulate cortex; PrL, prelimbic cortex; S1, primary somatosensory cortex. Colored bars in B, D and F reflect pixel intensity.

then incubated the sections overnight in an avidin–biotin–horseradish peroxidase conjugate (Vector Laboratories) and stained them with 0.05% 3,3′-diaminobenzidine tetrahydrochloride (Sigma), 0.02% H_2O_2, 0.05% cobalt chloride, and 0.01% nickel ammonium sulfate. Sections were then mounted onto slides, dehydrated, and coverslipped.

Statistical analysis

For analysis of the response rate of pyramidal (n = 19) and non-pyramidal (n = 17) neurons, we compared the proportions of responding and non-responding neurons of each type with Fisher's exact test (GraphPad).

Results

Rat GPe projections

In all six rats tested, tracer injections filled cell bodies and local fibers within the anterior GPe without filling cells in the BF (Figs 1 and 2A–C). Starting from the rostrocaudal level of the GPe, we observed, in all rats, innervation of Fr2, an anatomical region also known as the secondary motor cortex/frontal cortex, agranular medial cortex, medial precentral area, and secondary motor area (Uylings *et al.*, 2003). The projections were ipsilateral, passing through the striatum and terminating in Fr2 (Fig. 2A). Fr2 projections were sparse at the level of the injection, increased in density in rostral sections (Fig. 2B and C), and reached their greatest density at the rostral extent of the striatum (Fig. 2D). GPe projections reached the most rostral parts of the forebrain (Fig. 2E and F), spreading laterally in frontal regions while remaining sparse in the medial wall and orbital regions (Fig. 2F). Projections to Fr2 appeared to be topographic, with more lateral injections within the GPe producing more lateral projections to both the striatum and Fr2. However, projections always targeted Fr2 while avoiding the anterior cingulate cortex. No cell bodies were stained in the cortex.

To quantify the cortical projections, we inverted the grayscale images and measured the staining intensity of projections within cortical subregions in three representative coronal sections (Fig. 3). At a level anterior to the striatum (Fig. 3A and B), projections – including fibers and terminals – were heaviest in Fr2, followed by lighter staining in the adjacent primary motor cortex (M1) and cingulate cortex, some staining in the anterior insula, and almost no projections in the prelimbic or sensory cortices. At the anterior tip of the striatum (Fig. 3C and D), the heaviest staining was seen in Fr2, with staining also being seen in the adjacent M1 and anterior insula. Little or no staining was observed in the prelimbic, cingulate and sensory cortices. In the rostral striatum (Fig. 3E and F), staining was heaviest in Fr2, with some projections in M1 and the anterior insula, and little staining elsewhere. In general, heavier projections were seen in more anterior sections, and no cortical projections were seen caudal to the injection site.

Projections in Fr2 were densest in deep projection layer V of the cortex (Figs 3A, C and E and 4D), although terminal boutons were observed from the level of the injection site to the rostral extent of the cortex (see insets, Fig. 1A–F) in both superficial (Fig. 4B) and deep (Fig. 4C) layers. Dense GPe projections were observed in the STN, entopedunclear nucleus/GPi, SNr, and substantia nigra pars compacta (Fig. 4D–F), and in the striatum (Fig. 1A–C), consistent with previous reports of GPe projections (Kita, 2007). Bilateral projections, with ipsilateral predominance, were also observed in the reticular, mediodorsal, parafascicular and centrolateral nuclei of the thalamus (Fig. 4G).

Striatal projections to pallidocortical neurons

Neurons in the BF located ventral to the GPe have glutamatergic, GABAergic and cholinergic projections throughout the cortex (Saper, 1984; Gritti *et al.*, 1997; Henny & Jones, 2008), but these neurons do not receive striatal input. To differentiate GPe projections to the cortex from BF projections in the cortex, we injected a retrograde fluorogold tracer (stained brown) into Fr2 in six rats (Fig. 5A), along with, in two rats, an anterograde biotinylated dextran amine tracer (stained black) into the rostral dorsal striatum (Fig. 5B), which projects to the GPe but not to the BF. Consistent with ChR2 tracing of the pallidocortical pathway, we observed retrogradely labeled neurons throughout the GPe (see representative trace

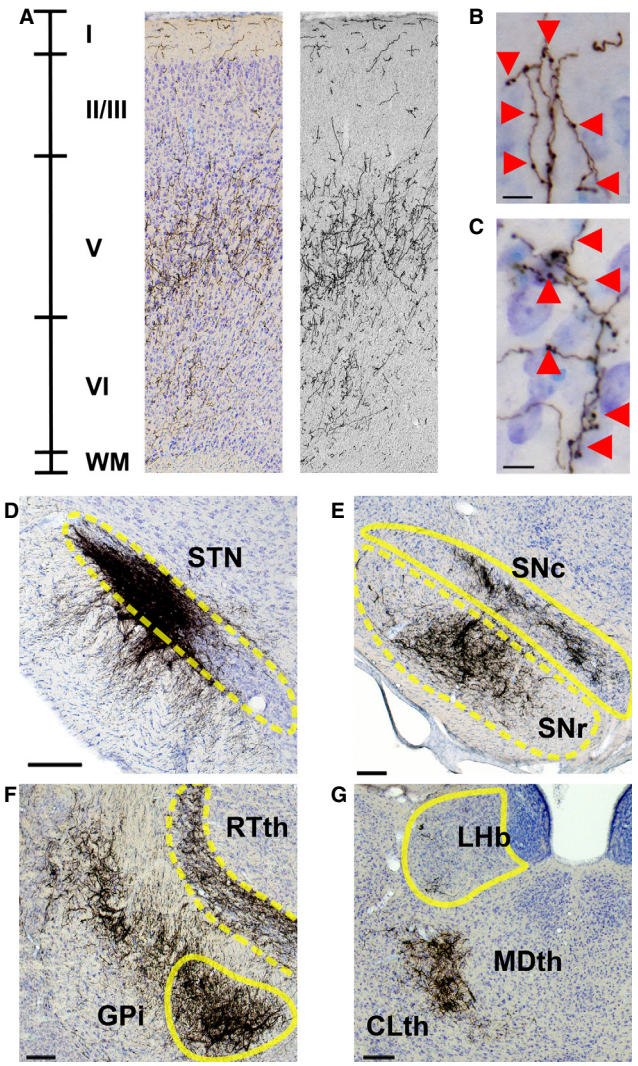

FIG. 4. Additional details of GPe projections to the cortex and other regions. (A) Fr2 projections from the GPe, showing a heavier concentration of projections to layers V and VI. (B) Closeup of pallidocortical boutons in layer I. (C) Closeup of pallidocortical boutons in layer V. (D–G) Projections from the GPe, shown by tracer injection into the GPe, to (D) the STN, (E) the substantia nigra pars compacta (SNc) and SNr, (F) the GPi and reticular thalamus (RTth), and (G) the lateral habenula (LHb) and thalamus, including the mediodorsal thalamus (MDth) and the centrolateral thalamus (CLth). Scale bars: 10 μm (B and C) and 100 μm (D–G).

in Fig. 5C) in all six rats, as well as neurons in the BF. In rats with anterograde tracing, neurons in the GPe also received projections from striatal neurons (Fig. 5D–H). Extended focus microscopy revealed striatal terminal boutons on cell bodies and dendrites of the GPe neurons that were retrogradely labeled from Fr2. Conversely, BF neurons ventral to the GPe did not receive any projections from the striatum (Fig. 5I).

Mouse GABA GPe projections

GPe neurons are mostly GABAergic, but non-GABAergic neurons, especially cholinergic GPe neurons, are thought to project to the cortex (Walker *et al.*, 1989; Moriizumi & Hattori, 1992). To differentiate the GABAergic GPe projections observed in the rats from cholinergic projections of the GPe (Saper, 1984), we injected cre-dependent EF1a–DIO–hChR2 (H134R)–eYFP–AAV10 into the GPe Vgat-ires-cre mice (Fig. 6A and B).

Consistent with rat pallidocortical projections, we observed, in all injected mice, GABAergic GPe fiber projections to Fr2, beginning near the rostrocaudal level of the GPe (see representative trace in Fig. 7A) and becoming heaviest at the level of the most rostral aspect of the striatum (Fig. 7B–D). Projections were also observed at the most rostral aspect of the forebrain, becoming sparser along the ventral medial wall (Fig. 7E and F). Notably, GABAergic BF neurons at this level project to the infralimbic (Henny & Jones, 2008) and somatosensory cortices (Gritti *et al.*, 1997); we did not observe similar innervation of the infralimbic or somatosensory cortices by GABAergic GPe neurons.

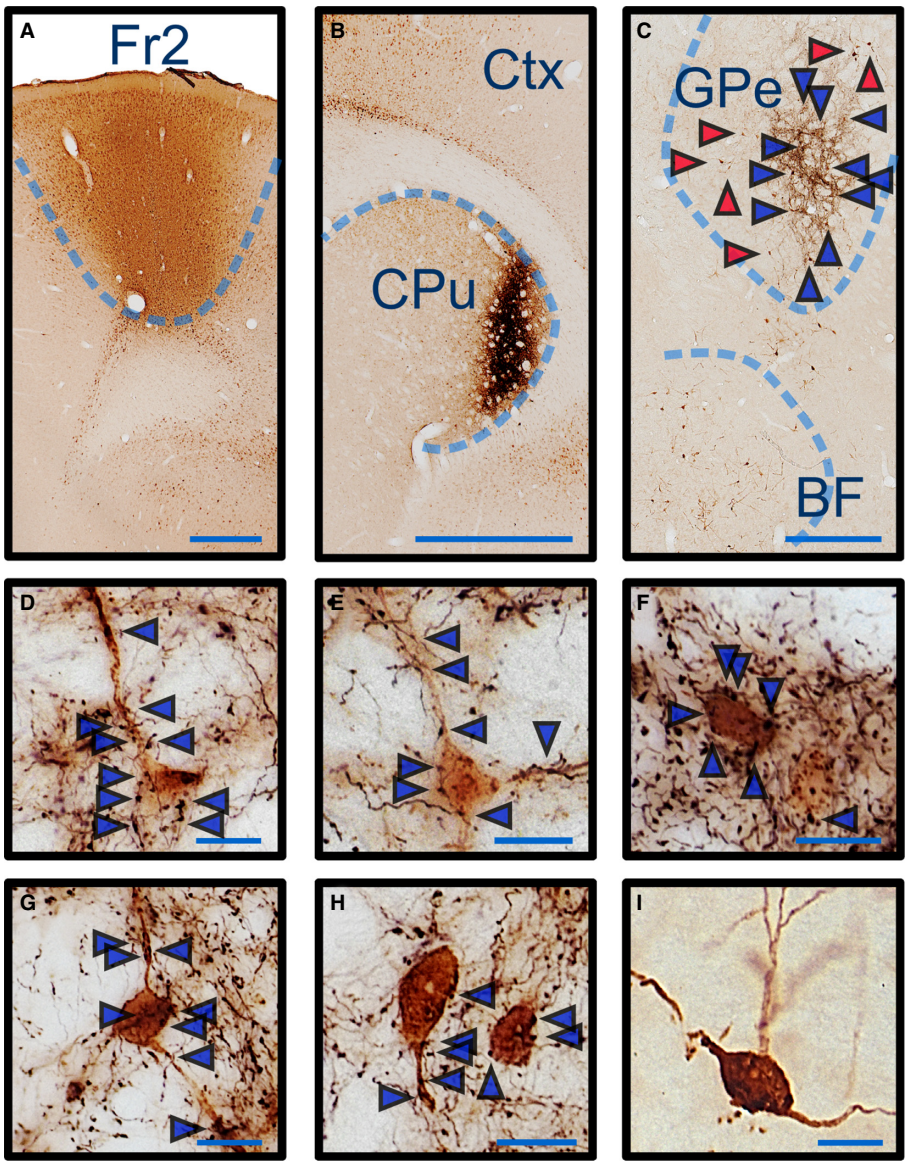

FIG. 5. Retrograde tracing from Fr2 with fluorogold, stained brown, labels GPe neurons that also receive anterograde tracing from the CPu with biotinylated dextran amine (BD), stained black. (A) Injection site of fluorogold, stained brown, into Fr2. (B) Injection site of BD, stained black, into the CPu. Cortical neurons retrogradely labeled from Fr2 are also visible throughout the cortex. (C) GPe and BF neurons retrogradely labeled from Fr2 fluorogold injections. Black fibers from CPu anterograde tracing converge on the GPe, but not on the BF. The restricted injection site in the CPu and the topographic projection from the CPu to the GPe reveal GPe neurons that project to the cortex and receive terminals from the CPu anterograde tracer (blue arrows), as well as GPe neurons that project to the cortex but are not targeted by the tracer (red arrows). (D–H) Extended focus imaging of GPe neurons retrogradely labeled from Fr2, stained brown, and black appositions from striatal inputs, stained black. CPu appositions target the cell body and dendrites of GPe neurons (blue arrows). (I) A BF neuron retrogradely labeled from Fr2, with no CPu anterograde input. CTx, cortex. Scale bars: 1 mm (A–C) and 20 μm (D–F).

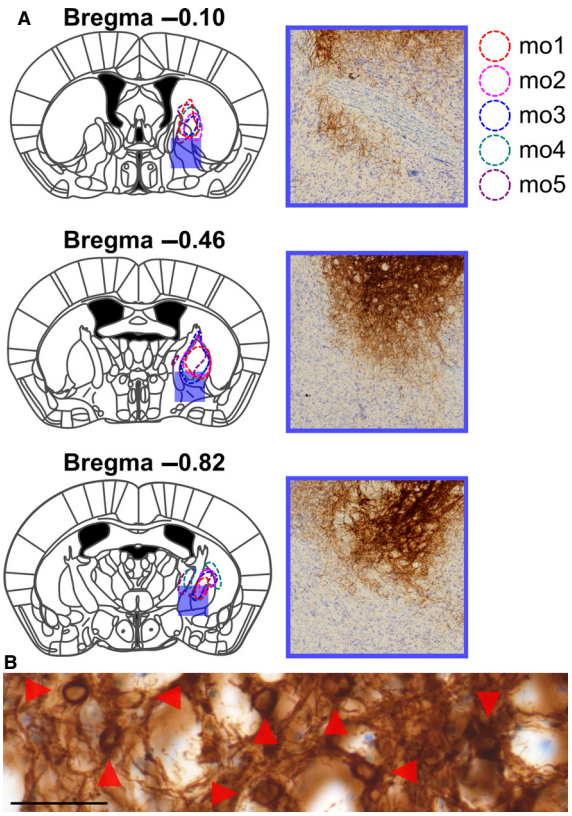

FIG. 6. Sites of injection of ChR2 into the mouse GPe overlaid onto a standard mouse atlas. (A) All injections were unilateral, and injection outlines are split between sides for visibility. Boxes, corresponding to case mo3, show a magnified image of the blue square zones on the injection diagram. Magnified images of the injection site in the GPe show extensive fibers, with no filled cell bodies, in the BF. (B) Filled cell bodies in the GPe injection site. Scale bar: 100 μm.

To quantify these GABAergic projections, we measured the staining intensity of projections – fibers and terminals – within cortical subregions in three representative coronal sections (Fig. 8). At a level anterior to the striatum (Fig. 8A and B), projections were heaviest in Fr2, followed by lighter staining in the cingulate cortex and M1, with few projections in the anterior insula or prelimbic and sensory cortices. At the anterior tip of the striatum (Fig. 8C and D), the heaviest staining was seen in Fr2, with staining also being seen in the adjacent M1 and cingulate cortex, and lighter or no staining in prelimbic, cingulate or sensory cortices. In the rostral striatum (Fig. 8E and F), staining was heaviest in Fr2, with some projections in M1, the cingulate cortex, and the anterior insula, and little staining elsewhere. In Fr2 and adjacent subregions, the most intense staining was seen in deeper, projection layers of the cortex, and, as in rats, heavier projections were seen in more anterior sections. No cortical projections were seen caudal to the injection site. As in rats, GPe fibers and boutons in Fr2 were heaviest in layers V and VI, although fibers and terminals were seen throughout all layers of the cortex (Fig. 9A–C). Also as in rats, GPe injections of DIO–hChR2–eEYP revealed fibers and terminals in the STN, EPN/GPi, SNr, and striatum, as well as in the mediodorsal, centrolateral, parafascicular and reticular thalamus (Fig. 9D–G).

In vitro *optogenetic characterisation of pallidocortical projections*

To confirm the presence of GABAergic pallidocortical projections, and to characterise the functional targets of these projections, we injected EF1a–DIO–hChR2 (H134R)–eYFP–AAV10 into the GPe of five Vgat-ires-cre-GFP mice. We recorded from GABAergic/GFP-expressing neurons and pyramidal neurons of layers V/VI of Fr2 (Fig. 10A), as these deep layers receive the strongest pallidocortical

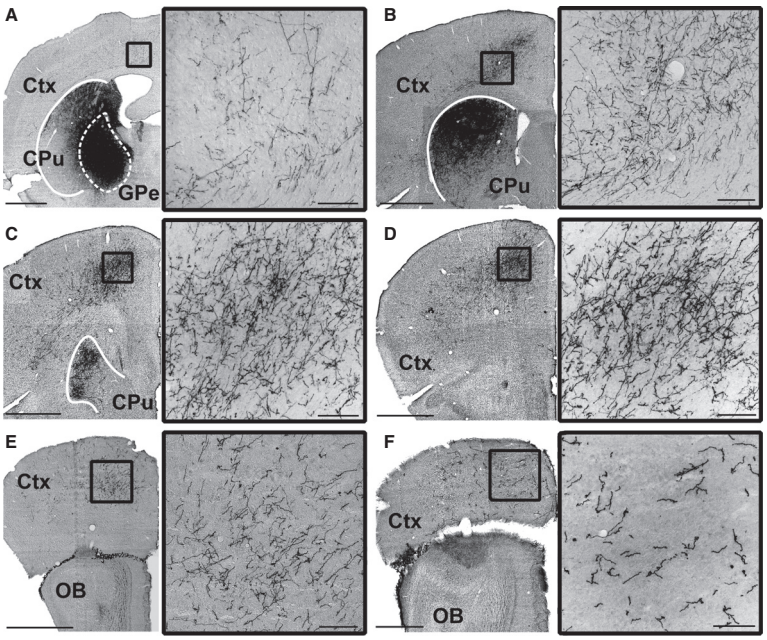

FIG. 7. Cre-dependent tracer injection into the GPe of Vgat-ires-cre mice, stained brown against YFP, label GABAergic projections to the Fr2 cortex at levels rostral to the injection site. (A) At the level of the injection site, heavy staining is seen in the dorsal striatum, whereas sparse projections and terminals can be seen passing through the corpus callosum into Fr2 (inset). (B) At the rostrocaudal level of the striatum, GPe projections into both the the striatum and Fr2 can be seen (inset). (C and D) GPe projections to Fr2 reach their heaviest level at the rostral extent of the striatum, with dense fibers and terminals throughout layers V and VI (insets). (E and F) GPe projections extend more laterally across the cortex in more rostral sections, while remaining sparse along the medial wall and orbital regions (E), and reach the most rostral extent of the cortex (F). CTx, cortex; OB, olfactory bulb. Data are presented for case mo3. Scale bars: 1 mm; insets 100 μm.

projections (Figs 3 and 8). Under IR visualisation, GABAergic/GFP-expressing neurons had a round soma quite distinctive from the neighboring pyramidal cells (Fig. 10B), were silent at resting membrane potential (−53.93 ± 2.6 mV), and had an input resistance of 208.18 ± 28.65 MΩ (n = 10). These neurons responded to depolarising current steps with fast and high-frequency firing (Fig. 10C). They also showed a narrow action potential (width, 0.61 ± 0.04 ms) followed by a large after hyperpolarisation (−19.53 ± 2.13 mV; n = 10). They responded to hyperpolarising pulses with a small, voltage-dependent rectification and a small depolarising sag, suggesting the presence of an inwardly rectifying I_K and an I_h.

Photostimulation of axons and terminals that originated from GPe^{Vgat} neurons evoked release of GABA, which inhibits the firing of GFP-positive Fr2 neurons. This effect was blocked by bicuculline (10 μM; Fig. 10D), indicating that these responses were mediated by activation of $GABA_A$ postsynaptic receptors. In voltage-clamp recordings, photostimulation of GPe^{Vgat} axons/terminals evoked fast IPSCs in GFP-positive Fr2 neurons (n = 10 of 17 neurons; Fig. 10E–I) that were completely abolished by bicuculline. The peak amplitude of the photoevoked IPSCs was 34.57 ± 11.3 pA, and IPSC rise and decay could be fitted with single exponentials (rise time constant, 1.9 ± 0.3 ms; decay time constant, 13.57 ± 1.98 ms) (Fig. 10H). Paired pulse tests (80-ms inter-pulse

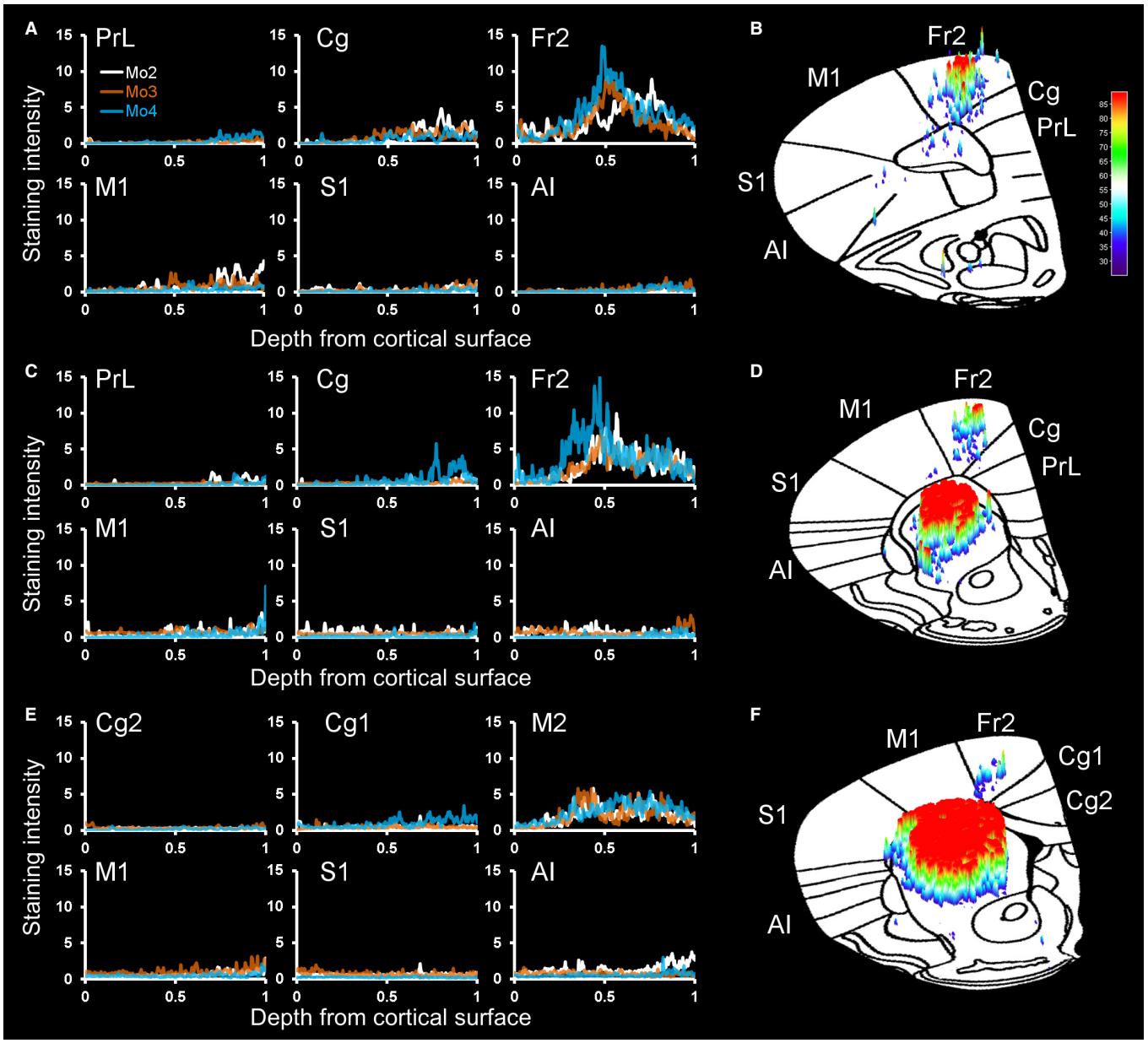

FIG. 8. Quantitative mapping of GPe projections to cortical subregions in Vgat-ires-cre mice. (A, C, and E) Projection mapping in three representative mice cases, with plotting of normalised staining intensity against relative distance from the cortical surface to the white matter. (B, D and F) Projection intensity from case mo4 overlaid on a standardised mouse atlas demonstrates the typical pattern of the GABAergic pallidocortical projection, with heavy projections to Fr2 and adjacent areas. Staining intensities of six major cortical areas are presented at the level anterior to the striatum (A and B), the anterior striatum (C and D), and the striatum (E and F). AI, anterior insula; Cg, cingulate cortex; PrL, prelimbic cortex; S1, primary somatosensory cortex. Colored bars in B, D and F reflect pixel intensity.

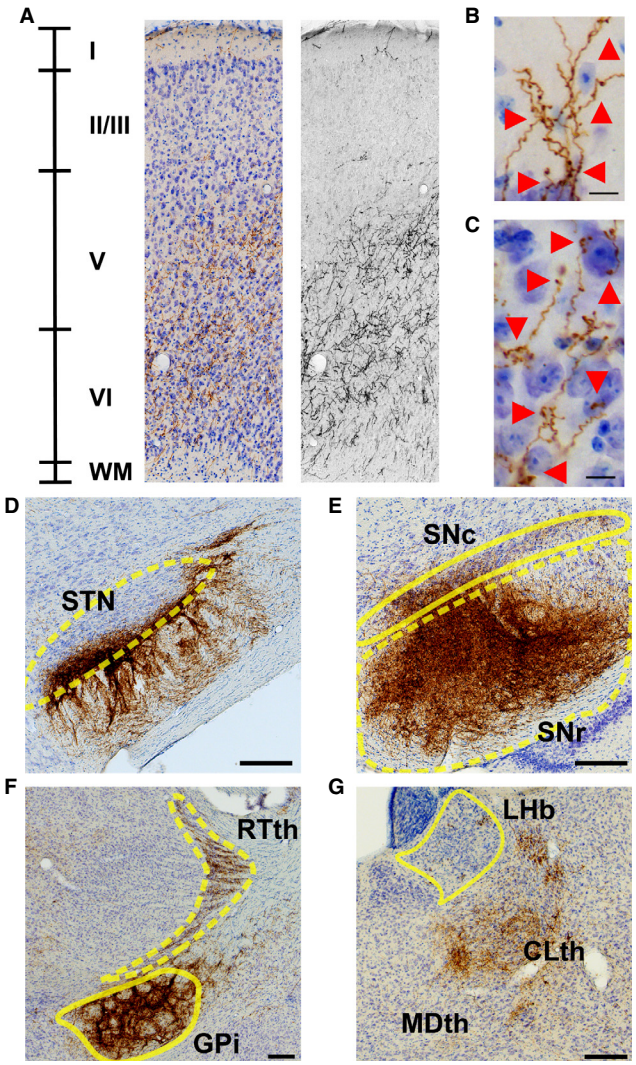

FIG. 9. Additional details of GPe projections to the cortex and other regions. (A) Fr2 projections from the GPe, showing a heavier concentration of projections to layers V and VI. (B) Closeup of pallidocortical boutons in layer I. (C) Closeup of pallidocortical boutons in layer V. (D–G) Projections from the GPe, shown by tracer injection into the GPe, to (D) the STN, (E) the substantia nigra pars compacta (SNc) and SNr, the (F) GPi and reticular thalamus (RTth), and (G) the lateral habenula (LHb) and thalamus, including the mediodorsal thalamus (MDth) and the centrolateral thalamus (CLth). Scale bars: 10 μm (B and C) and 100 μm (D–G).

intervals) showed robust paired pulse depression (76%; $n = 2$), suggesting high release probability of GPe^{Vgat}→Fr2^{GFP+} input (Fig. 10I). In addition, the onset delay of the photo-evoked IPSCs was short (4.38 ± 0.28 ms; Fig. 10G), supporting direct synaptic connectivity from GPe to Fr2 GABAergic interneurons.

We also recorded from 19 pyramidal cells in the same layers of the Fr2 cortex. These neurons were identified on the basis of their shape and their firing properties (Fig. 10J and K). Photostimulation of GPe^{Vgat} axons and terminals evoked IPSCs in three of 19 pyramidal neurons (Fig. 10L). The peak amplitude of the photo-evoked IPSCs in these three pyramidal cells was 15.4 ± 6.2 pA, and, importantly, the onset delay of the photo-evoked IPSCs was short (5.19 ± 0.62 ms), supporting direct synaptic connectivity from GPe to Fr2 pyramidal cells.

Overall, optogenetic activation of GPe^{Vgat} projections evoked inhibitory synaptic responses in a greater proportion of Fr2 GABAergic neurons (58.8%) than Fr2 pyramidal neurons (15.8%; Fisher's exact test, $P = 0.01$). These results indicate that functional GPe^{Vgat} projections target Fr2 neurons, primarily GABAergic interneurons and some pyramidal cells.

Discussion

Using a ChR2-based tracer in rats, we found ipsilateral projections from the GPe to all cortical layers, especially to the pyramidal cell-containing layer V, of Fr2, also known as the secondary motor cortex or M2. We confirmed that these are GPe neurons by retrogradely labeling from Fr2 in combination with anterograde labeling from the

FIG. 10. Photostimulation of GP^{Vgat} projections evoke GABA release onto Fr2 GABAergic interneurons. (A) Scheme of a coronal recording slice containing Fr2 cortex and the location of our recordings. (B) Photomicrographs showing GFP-positive neurons in layers V and VI from a Vgat-ires-cre-GFP mouse (left), and visualised under an IR differential interference contrast system during whole cell recordings (right) (scale bar: 50 μm). (C) Firing properties in response to depolarising and hyperpolarising current steps of a representative GFP-positive neuron that responded to photostimulation of the GP^{vgat} projections. These neurons respond to depolarising current steps (+300 pA, from –75 mV; top trace) with fast and high-frequency firing and with a large after hyperpolarisation, and they respond to hyperpolarising pulses (–20 pA, from –40 mV; bottom traces) with a small, voltage-dependent rectification and a small depolarising sag, suggesting the presence of an inwardly rectifying I_K and an I_h (scale bars: 20 mV and 200 ms) (dashed line: 0 mV). (D) Photostimulation of ChR2-expressing GPe^{Vgat} axons evokes GABA release and inhibits action potential firing of GFP-positive neurons of the Fr2 cortex, and this effect is blocked by bicuculline methiodide (10 μM). Action potentials are evoked by 5-ms current pulses (80 pA). (E) In voltage-clamp recordings, photostimulation evokes $GABA_A$-mediated IPSCs in Fr2 GFP-positive neurons. Photo-evoked IPSCs (average of 25 trials) were recorded at –40 mV in control artificial cerebrospinal fluid (Con), in bicuculline (Bic), and following wash-out of bicuculline (wash). (F) A representative raster plot of IPSCs (left panel; 50-ms bin) and average IPSC probability in all recorded Fr2 GFP-positive neurons following photostimulation of the GPe^{Vgat}→Fr2^{GFP+} pathway (right panel; 50-ms bin; $n = 17$ neurons; SEM). (G) Onset delay of $GABA_A$-mediated IPSCs in Fr2 GFP-positive neurons ($n = 10$; mean ± SEM in red). (H) Photo-evoked IPSC decay was fitted with a single exponential (gray, average IPSCs from 30 traces; black dotted trace, single exponential fits correlation coefficient = 0.995; weighted decay time constant = 9.67 ms). (I) Paired pulse test (80-ms inter-light pulse interval) showed significant paired pulse depression of the photo-evoked IPSCs in Fr2 GFP-positive neurons (left panel; gray traces, 20 trials; black trace, average IPSCs). A summary graph (right panel; 40 trials from two neurons) is shown. IPSCs are normalised over the average first-pulse IPSC amplitude (mean ± SEM in red). (J) Two representative pyramidal cells that did not respond to photostimulation of the GP^{vgat}, one visualised under an IR differential interference contrast system system during whole cell recordings (top panel) (scale bar: 20 μm) and one labeled with avidin–biotin–horseradish peroxidase conjugate/3,3′-diaminobenzidine tetrahydrochloride nickel staining of biocytin injected during whole cell recordings (bottom panel) (scale bar: 50 μm) (K) These neurons show the typical firing properties of cortical pyramidal cells, including fast initial adaptation followed by a regular firing pattern (top trace; depolarising current pulses +120 pA, from –65 mV) (scale bar: 20 mV and 200 ms) (dashed line: 0 mV), significant voltage-dependent rectification, and a small depolarising sag, suggesting the presence of a large, inwardly rectifying I_K and a small I_h (bottom traces; hyperpolarising current pulses –40 pA, from –60 mV) (scale bar: 20 mV and 200 ms) (dashed line: 0 mV). (L) The majority of Fr2 pyramidal cells did not respond to photostimulation (16 of 19 recorded Fr2 pyramidal cells). A representative raster plot of IPSCs in an Fr2 pyramidal cell (left panel; 50-ms bin) and average IPSC probability in all recorded Fr2 pyramidal cells following photostimulation of the GPe^{Vgat}→Fr2^{pyramidal} pathway (right panel; 50-ms bin; $n = 19$ pyramidal cells; SEM) are shown. In all of the recordings, we used 5-ms blue-light pulses, indicated by blue bars at the top or the bottom of the recording traces.

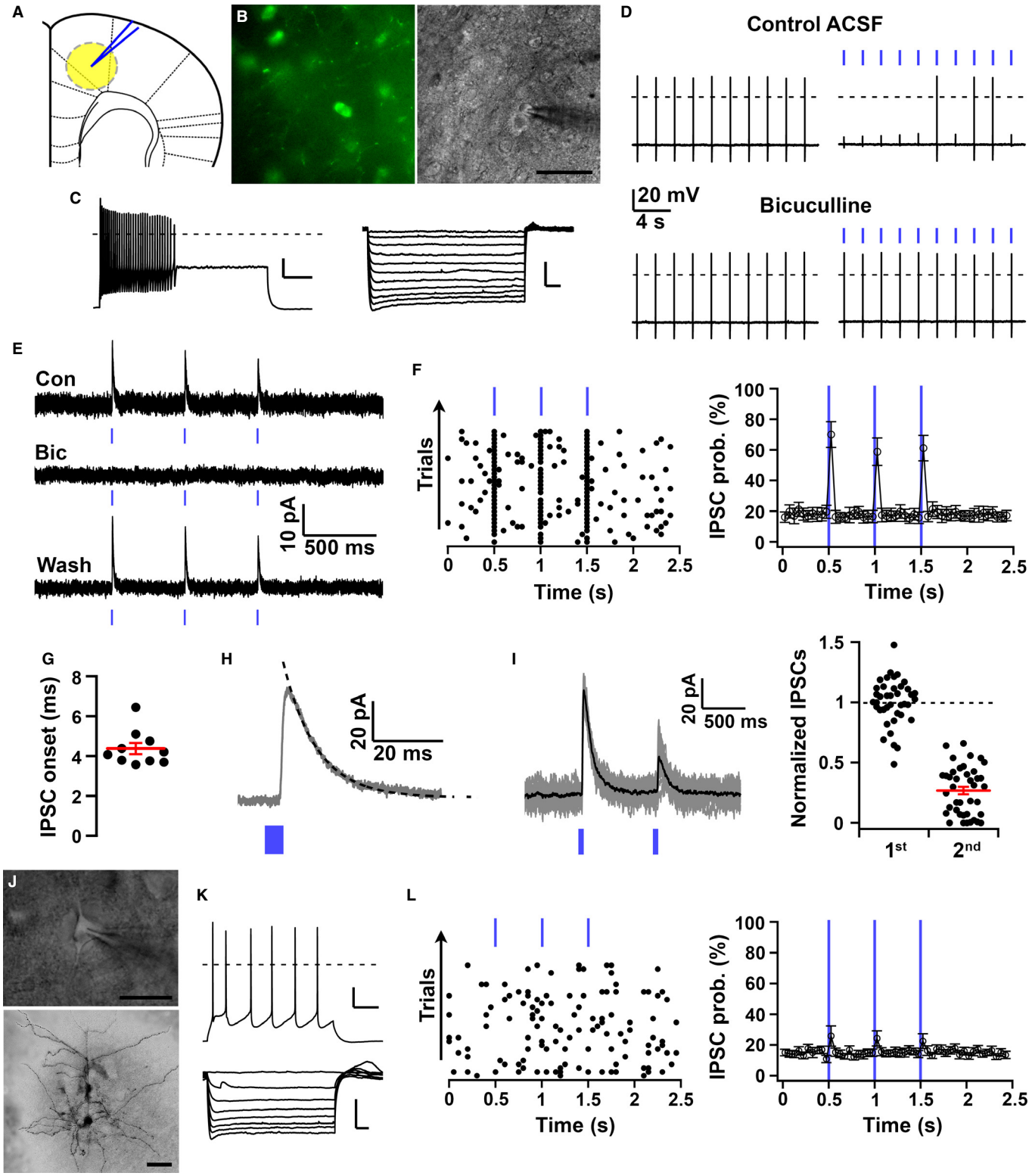

CPu, revealing cortically projecting GPe neurons innervated by the CPu. We then showed, by using Vgat-ires-cre mice, that these GPe projections to the cortex are GABAergic. Finally, we confirmed by using *in vitro* optogenetic stimulation that these GABAergic pallidocortical projections can target neurons in the cortex and produce a rapid, inhibitory synaptic response that inhibits action potential firing. Taken together, these findings suggest that the GPe and, by extension the basal ganglia, project directly to the cortex. Although previous studies have retrogradely labeled neurons in the GPe from the cortex (Van Der Kooy & Kolb, 1985), it was unclear whether these projections originated from GPe neurons rather than BF neurons, whether these projections targeted a specific cortical region, and whether stimulation of this projection directly affected cortical neurons. The present study is the first to show that the cortically projecting GPe neurons receive striatal projections, and thus form part of a basal ganglia system that projects directly to the prefrontal cortex, especially

the deep layers of Fr2. Furthermore, the present study is the first to characterise a functional, inhibitory role of GABAergic pallidocortical projections on cortical neurons. This pallidocortical projection is a unique pathway for basal ganglia–cortical interaction.

Pallidocortical projections allow GABAergic neurons of the GPe, which receive projections from all basal ganglia input and output nuclei, to directly influence cortical activity. Quantification of staining intensity confirmed that the heaviest projection density is in Fr2, with some additional projections in the adjacent cingulate and motor cortices – two regions immediately adjoining Fr2 – as well as the anterior insula. The projection field is wider in the most rostral parts of the prefrontal cortex, where the precise delineation of Fr2 and other regions is unclear (Uylings *et al.*, 2003). In contrast, the GPe does not send heavy projections to orbital, infralimbic, prelimbic or sensory regions, and nor do projections target motor or premotor regions caudal to the injection site, although the caudal GPe may have additional cortical targets. Just as CPu anterograde tracing targeted a specific region of the GPe, cortically projecting GPe neurons target Fr2 in the rostral cortex and striatum in a topographic manner. GPe projections to the cortex, basal ganglia and thalamus (Gandia *et al.*, 1993) enable the GPe to influence multiple circuits throughout the brain.

Fr2 has been compared with the frontal cortex of primates, although there is debate concerning the precise mapping of homologous primate and rodent frontal regions (Preuss, 1995; Uylings *et al.*, 2003; Wise, 2008). The Fr2 region has been specifically implicated in a range of functions, particularly those shaping the selection and initiation of action (Grillner *et al.*, 2005; Sul *et al.*, 2011). Much as the GPe is a hub of basal ganglia activity, Fr2 receives input from somatosensory and other cortical regions (Condé *et al.*, 1995) while projecting to the motor cortex. Through the pallidocortical pathway, the GPe is probably able to play a direct role in behavior, such as modulation of Fr2 activity to adapt to reward contingencies (Kargo *et al.*, 2007). Because GPe projections to other cortical regions are so limited, we hypothesise that the pallidocortical pathway is a specialised circuit for the regulation of premotor and motor activity. In contrast, other cortically projecting systems, such as the BF, project widely throughout the cortex and modulate global patterns of cortical activity. The pallidocortical pathway bridges two regions that, in turn, integrate inputs and outputs from the basal ganglia and cortex, respectively. This direct shortcut from the basal ganglia to the cortex may play a specialised role alongside basal ganglia–thalamic–cortical loops.

Our *in vitro* experiments indicate that the pallidocortical pathway preferentially targets GABAergic neurons in Fr2, presumably interneurons. These putative interneurons had firing properties resembling those of fast-spiking GABAergic/parvalbumin-positive cortical interneurons (Cauli *et al.*, 1997) which account for almost 50% of neocortical GABAergic cells in layers V and VI (Rudy *et al.*, 2011). We also found that the GPe projects to pyramidal cells, although the proportion of responding pyramidal neurons is less than that of GABAergic neurons. Also, although we focused on deep layer projections, pallidocortical projections to superficial layers may also contribute to GPe modulation of cortical activity. GPe neurons may help set cortical firing rates via direct input to cortical interneurons as well as indirect input to pyramidal cells or via the indirect basal ganglia pathway. Future work must delineate the molecular and physiological properties of the origins and targets of pallidocortical neuron projections, both within the known organisation of GPe neurons (Nóbrega-Pereira *et al.*, 2010; Mallet *et al.*, 2012; Mastro *et al.*, 2014) and within the cortical architecture.

Cholinergic and GABAergic BF neurons project widely throughout the cortex, sharing many developmental, anatomical and functional characteristics with the GPe. Retrograde tracing studies from Fr2 show projections originating not only from BF populations but also from within the GPe itself (Zaborszky *et al.*, 2013). Unlike output from BF neurons, which project diffusely across the cortex, output from the GABAergic pallidocortical pathway is concentrated on Fr2 and avoids other BF targets, including the amygdala and lateral hypothalamus. Although our retrograde tracing from Fr2 reveals BF innervation of the cortex, these neurons – which are located ventrally to the GPe – did not receive projections from the CPu. The BF and GPe both contain GABA neurons that project to the cortex, and appear to form a continuous population, based on retrograde tracing alone, especially at caudal levels, but only GPe neurons receive striatal input as part of the basal ganglia system. Delineating the similarities and differences between GPe and BF physiology and anatomy will be critical to understanding how the basal ganglia and BF interact with the cortex. For example, although our *in vitro* experiments clearly indicate that the pallidocortical pathway has a GABAergic, inhibitory phenotype, the cholinergic neurons within the GPe may also contribute a cortical projection, although these neurons are sparse within the GPe at the rostral levels that we examined (Walker *et al.*, 1989; Moriizumi & Hattori, 1992). It is unclear whether these cholinergic neurons within the GPe or in the borders of the GPe receive CPu inputs.

In summary, we describe a GABAergic pallidocortical output pathway that directly links the basal ganglia and cortex. The rapid and inhibitory response produced by *in vitro* stimulation of pallidocortical terminals supports a role for the GPe in shaping Fr2 firing patterns. Direct inhibitory GABAergic projections from the GPe to the projecting layers of the Fr2 cortex may disinhibit premotor regions to influence motor planning and execution (Kargo *et al.*, 2007) or provide a direct route for the propagation of deleterious basal ganglia oscillations to the cortex, such as the abnormal oscillations in GPe–STN circuits present in Parkinson's disease (Mallet *et al.*, 2008; Obeso *et al.*, 2008). The identification of this pallidocortical circuit may provide a structural basis for understanding the pathological motor features of basal ganglia disorders, and suggests an important role for GPe–cortical dialogue in motor control.

Acknowledgements

The authors thank Quan Ha and Xi Chen for technical expertise. This work was supported by the Hilda and Preston Davis Foundation (M. C. Chen) and National Institutes of Health (NS061863, NS082854 and HL095491 to E. Arrigoni; NS073613 to P. M. Fuller; NS062727 and NS061841 to J. Lu). The authors report no conflict of interest.

Abbreviations

AAV, adeno-associated viral vector; BF, basal forebrain; ChR2, channelrhodopsin-2; CPu, caudate putamen; DIO, double-floxed inverse ORF; EF1a, elongation factor-1 alpha; eYFP, enhanced yellow fluorescent protein; Fr2, frontal area 2; GFP, green fluorescent protein; GPe, globus pallidus externa; GPi, globus pallidus interna; hChR2, humanised channelrhodopsin-2; IPSC, inhibitory postsynaptic current; IR, infrared; M1, primary motor cortex; SEM, standard error of the mean; SNr, substantia nigra reticulata; STN, subthalamic nucleus; YFP, yellow fluorescent protein.

References

Albin, R.L., Young, A.B. & Penney, J.B. (1989) The functional anatomy of basal ganglia disorders. *Trends Neurosci.*, **12**, 366–375.

Cauli, B., Audinat, E., Lambolez, B., Angulo, M.C., Ropert, N., Tsuzuki, K., Hestrin, S. & Rossier, J. (1997) Molecular and physiological diversity of cortical nonpyramidal cells. *J. Neurosci.*, **17**, 3894–3906.

Condé, F., Maire-Lepoivre, E., Audinat, E. & Crépel, F. (1995) Afferent connections of the medial frontal cortex of the rat. II. Cortical and subcortical afferents. *J. Comp. Neurol.*, **352**, 567–593.

Fasano, A., Daniele, A. & Albanese, A. (2012) Treatment of motor and non-motor features of Parkinson's disease with deep brain stimulation. *Lancet Neurol.*, **11**, 429–442.

Franklin, K.B.J. & Paxinos, G. (2008) *The Mouse Brain in Stereotaxic Coordinates*. Academic Press, San Diego, CA.

Fuller, P.M., Fuller, P., Sherman, D., Pedersen, N.P., Saper, C.B. & Lu, J. (2011) Reassessment of the structural basis of the ascending arousal system. *J. Comp. Neurol.*, **519**, 933–956.

Gandia, J.A., De Las Heras, S., García, M. & Giménez-Amaya, J.M. (1993) Afferent projections to the reticular thalamic nucleus from the globus pallidus and the substantia nigra in the rat. *Brain Res. Bull.*, **32**, 351–358.

Grillner, S., Hellgren, J., Ménard, A., Saitoh, K. & Wikström, M.A. (2005) Mechanisms for selection of basic motor programs – roles for the striatum and pallidum. *Trends Neurosci.*, **28**, 364–370.

Gritti, I., Mainville, L., Mancia, M. & Jones, B.E. (1997) GABAergic and other noncholinergic basal forebrain neurons, together with cholinergic neurons, project to the mesocortex and isocortex in the rat. *J. Comp. Neurol.*, **383**, 163–177.

Henny, P. & Jones, B.E. (2008) Projections from basal forebrain to prefrontal cortex comprise cholinergic, GABAergic and glutamatergic inputs to pyramidal cells or interneurons. *Eur. J. Neurosci.*, **27**, 654–670.

Kargo, W.J., Szatmary, B. & Nitz, D.A. (2007) Adaptation of prefrontal cortical firing patterns and their fidelity to changes in action–reward contingencies. *J. Neurosci.*, **27**, 3548–3559.

Kita, H. (2007) Globus pallidus external segment. *Prog. Brain Res.*, **160**, 111–133.

Mallet, N., Pogosyan, A., Márton, L.F., Bolam, J.P., Brown, P. & Magill, P.J. (2008) Parkinsonian beta oscillations in the external globus pallidus and their relationship with subthalamic nucleus activity. *J. Neurosci.*, **28**, 14245–14258.

Mallet, N., Micklem, B.R., Henny, P., Brown, M.T., Williams, C., Bolam, J.P., Nakamura, K.C. & Magill, P.J. (2012) Dichotomous organization of the external globus pallidus. *Neuron*, **74**, 1075–1086.

Mastro, K.J., Bouchard, R.S., Holt, H.A.K. & Gittis, A.H. (2014) Transgenic mouse lines subdivide external segment of the globus pallidus (GPe) neurons and reveal distinct GPe output pathways. *J. Neurosci.*, **34**, 2087–2099.

Moriizumi, T. & Hattori, T. (1992) Separate neuronal populations of the rat globus pallidus projecting to the subthalamic nucleus, auditory cortex and pedunculopontine tegmental area. *Neuroscience*, **46**, 701–710.

Nóbrega-Pereira, S., Gelman, D., Bartolini, G., Pla, R., Pierani, A. & Marín, O. (2010) Origin and molecular specification of globus pallidus neurons. *J. Neurosci.*, **30**, 2824–2834.

Obeso, J.A., Marin, C., Rodriguez-Oroz, C., Blesa, J., Benitez-Temiño, B., Mena-Segovia, J., Rodríguez, M. & Olanow, C.W. (2008) The basal ganglia in Parkinson's disease: current concepts and unexplained observations. *Ann. Neurol.*, **64**(Suppl 2), S30–S46.

Paxinos, G. & Watson, C. (2005) *The Rat Brain in Stereotaxic Coordinates*. 5th Edn. Elsevier Academic Press, Burlington, MA, USA.

Preuss, T.M. (1995) Do rats have prefrontal cortex? The Rose–Woolsey–Akert program reconsidered. *J. Cognitive Neurosci.*, **7**, 1–24.

Qiu, M.-H., Vetrivelan, R., Fuller, P.M. & Lu, J. (2010) Basal ganglia control of sleep–wake behavior and cortical activation. *Eur. J. Neurosci.*, **31**, 499–507.

Rudy, B., Fishell, G., Lee, S. & Hjerling-Leffler, J. (2011) Three groups of interneurons account for nearly 100% of neocortical GABAergic neurons. *Dev. Neurobiol.*, **71**, 45–61.

Saper, C.B. (1984) Organization of cerebral cortical afferent systems in the rat. II. Magnocellular basal nucleus. *J. Comp. Neurol.*, **222**, 313–342.

Sul, J.H., Jo, S., Lee, D. & Jung, M.W. (2011) Role of rodent secondary motor cortex in value-based action selection. *Nat. Neurosci.*, **14**, 1202–1208.

Uylings, H.B.M., Groenewegen, H.J. & Kolb, B. (2003) Do rats have a prefrontal cortex? *Behav. Brain Res.*, **146**, 3–17.

Van Der Kooy, D. & Kolb, B. (1985) Non-cholinergic globus pallidus cells that project to the cortex but not to the subthalamic nucleus in rat. *Neurosci. Lett.*, **57**, 113–118.

Vitek, J.L., Zhang, J., Hashimoto, T., Russo, G.S. & Baker, K.B. (2012) External pallidal stimulation improves parkinsonian motor signs and modulates neuronal activity throughout the basal ganglia thalamic network. *Exp. Neurol.*, **233**, 581–586.

Vong, L., Ye, C., Yang, Z., Choi, B., Chua, S. Jr. & Lowell, B.B. (2011) Leptin action on GABAergic neurons prevents obesity and reduces inhibitory tone to POMC neurons. *Neuron*, **71**, 142–154.

Walker, R.H., Arbuthnott, G.W. & Wright, A.K. (1989) Electrophysiological and anatomical observations concerning the pallidostriatal pathway in the rat. *Exp. Brain Res.*, **74**, 303–310.

Wise, S.P. (2008) Forward frontal fields: phylogeny and fundamental function. *Trends Neurosci.*, **31**, 599–608.

Zaborszky, L., Csordas, A., Mosca, K., Kim, J., Gielow, M.R., Vadasz, C. & Nadasdy, Z. (2013) Neurons in the basal forebrain project to the cortex in a complex topographic organization that reflects corticocortical connectivity patterns: an experimental study based on retrograde tracing and 3D reconstruction. *Cereb. Cortex*, **25**, 118–137.